

The Optimal Use of Silicon Pixel Charge Information for Particle Identification

Harley Patton¹ and Benjamin Nachman²

¹*Computer Science Division, University of California, Berkeley*

²*Physics Division, Lawrence Berkeley National Laboratory*

June 17, 2022

Abstract

Particle identification using the energy loss in silicon detectors is a powerful technique for probing the Standard Model (SM) as well as searching for new particles beyond the SM. Traditionally, such techniques use the truncated mean of the energy loss on multiple layers, in order to mitigate heavy tails in the charge fluctuation distribution. We show that the optimal scheme using the charge in multiple layers significantly outperforms the truncated mean. Truncation itself does not significantly degrade performance and the optimal classifier is well-approximated by a linear combination of the truncated mean and truncated variance.

1 Introduction

Charged hadron identification plays a key role in many collider-based particle and nuclear physics analyses. For example, the ATLAS [1,2], CMS [3,4], and ALICE [5,6] experiments¹ at the Large Hadron Collider (LHC) can use the ionization energy loss (dE/dx) in silicon² from charged-particle trajectories to classify particles at low momentum ($\beta\gamma \lesssim 1$). This particle identification capability has been used to study properties of hadronization [12,13], including the effects of Bose-Einstein correlations [14] as well as to search for massive long lived unstable particles (LLPs), highly ionizing particles (HIPs), and heavy stable charged particles (HSCPs) [15–23] that are predicted in many theories of physics beyond the Standard Model.

¹The LHCb experiment [7] measures ionization in silicon from charged-particle tracks passing through their VELO detector [8]. This information is used for improving the position resolution [9] but only exploratory work exists for using it for particle identification [10].

²Ionization energy loss can be measured in other systems as well, for instance demonstrated in straw tubes in the ATLAS experiment’s Transition Radiation Tracker (TRT) [11]. The ideas discussed in this paper apply also to these other applications, but for focus the discussion here is restricted to silicon.

Particles with low $\beta\gamma$ or high electric charge can deposit significantly more energy than minimum ionizing particles (MIPs), with the average charge³ following the Bethe equation:

$$\left\langle -\frac{dE}{dx} \right\rangle \approx \frac{0.35}{\beta^2} [8.7 + 2 \log(\beta\gamma) - \beta^2] \text{ MeV / cm.} \quad (1)$$

Quoted values of dE/dx often divide by the density $\rho \approx 2.3 \text{ g/cm}^3$ to report a value in $\text{MeV cm}^2 / \text{g}$. For example, with a momentum of 500 MeV, the relative average dE/dx of protons, kaons, and pions are 3, 1.5, 1, respectively.

A key challenge with dE/dx -based particle-identification is that the energy loss probability distribution has significant and asymmetric fluctuations (‘straggling’). As a result of the skewed energy loss fluctuations (approximately Landau-distributed), the mean energy loss is much higher than the most probable energy loss. In addition to causing primary energy loss, ionized electrons can also have sufficient energy to cause further energy loss by ionization or excitation (δ -rays or knock-out electrons). These δ -rays are slow moving and highly ionizing, especially near their Bragg peak. For a complete review of energy loss fluctuations in silicon, see e.g. Ref. [24, 25]. To overcome the challenge of a significantly different energy loss straggling mean and mode, dE/dx -based methods combine information from multiple silicon layers and traditionally have used a truncated mean to approximate the mode of the charge distribution [1–6, 12–23]. Truncating and only using the average both remove information that may be useful for particle identification. The purpose of this paper is to study how much information, if any, is lost by these two standard data reduction schemes.

This paper is organized as follows. Section 2 introduces the simulation framework, and existing methods based on the truncated mean are illustrated in Sec. 3. The improvements from using all of the charge information are demonstrated in Sec. 4. The paper ends with some conclusions in Sec. 5.

2 Simulation

For concreteness, a detector setup similar to the ATLAS pixel detector is used for illustration. There are four pixel layers, each $200 \mu\text{m}$ thick with a pitch of $50 \times 250 \mu\text{m}^2$. Particles of a given momentum are incident perpendicular to the pixel surface⁴. Detector geometry and particle propagation are simulated using Allpix [26], built on the Geant4 package [27]. The setup is identical to the one described in Ref. [28] and is summarized here for completeness. Charge depositions and fluctuations are provided by Geant4 using the EMSTANDARD_OPT0 model⁵. The ionization energy is converted into electron-hole pairs and electrons are transported to the collecting electrode, including drift and diffusion. The diffusion length scales with the

³There is a significant difference between the mean and mode; the mode contains more information about the particle identity. For a comprehensive review about this topic and corrections to Eq. 1, see e.g. Ref. [24, 25].

⁴Charge fluctuations depend on the sensor thickness. Since the path length in silicon is the same for all particles in this study, this effect is removed. Future work could study the improvements to dE/dx -based tagging with variable path lengths (incidence angles) and adding thickness as a discriminating feature.

⁵This is not an accurate model for thin sensors, but $200 \mu\text{m}$ are sufficiently thick that the total deposited charge is well-modeled [29].

square-root of the drift time [30] and the diffusion constant is modeled according to the Einstein relation [31–33]. Electron and hole mobilities are parameterized using the common Canali-modified Caughey and Thomas velocity saturation model [34, 35]. The temperature is set to 273 K. In addition to diffusion, charges are deflected in a 2 T magnetic field that is perpendicular to the sensor depth. The angle of deflection is the Lorentz angle, given by $\tan \theta = r\mu B$. Deposited energy is digitized using a the time-over-threshold (ToT) method, with a linear conversion. The analog threshold is 3000 electrons, there are 8 bits of ToT, and a minimum ionizing particle (MIP) at perpendicular incidence corresponds to a ToT of 128 (half of the available range). The ToT is then converted to dE/dx by assuming 80 e/h pairs per micron for a MIP and 3.6 eV per e/h pair. Figure 1 shows the pixel cluster dE/dx distribution as a function of particle momentum for pions, kaons, and protons. Since protons are more massive than kaons which are more massive than pions, the proton dE/dx is shifted to higher values than kaons which is shifted to higher values than pions. For illustration, the next sections will focus on the kaon-versus-pion classification task; protons will also be discussed at the end of Sec. 4.

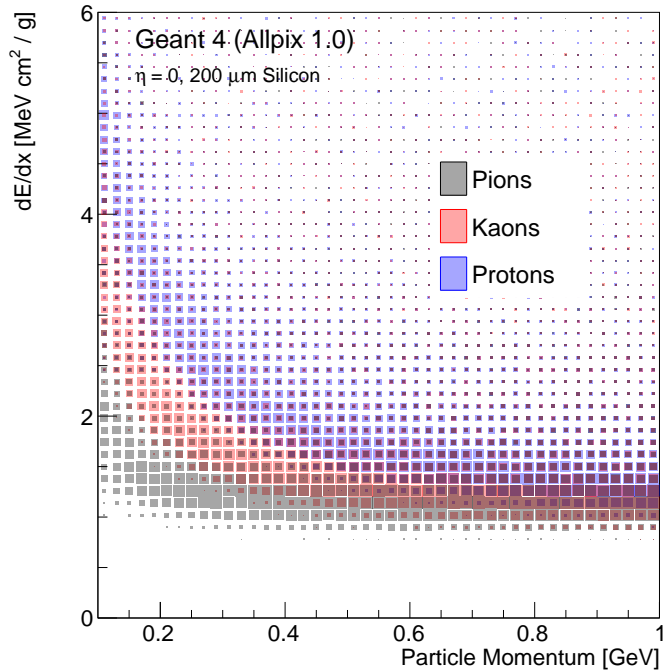


Figure 1: The distribution of the pixel cluster dE/dx as a function of the particle momentum for pions, kaons, and protons.

3 Existing Methods

For n dE/dx measurements $\{Q_i\}_{i=1..n}$, the truncated mean μ_t is simply the average over all the values, excluding $\max_i Q_i$. If more than two Q_i are the maximum, then multiple Q_i are discarded. This is the most standard approach to dE/dx-based charge identification. The reasoning behind this choice is that the energy loss in each detector layer is nearly Landau-distributed, with a very heavy tail that carries little to no discriminatory power. The left plot of Fig. 2 shows the dE/dx distribution for pions and kaons with $p = 400$ MeV. As expected, the kaon distribution is shifted to the right of the pion distribution because $\beta\gamma$ is lower for the kaons due to their higher mass. The right plot of Fig. 2 shows the likelihood ratio of kaons to pions. Where the likelihood ratio is not unity, the distribution has significant discrimination power. Beyond dE/dx ~ 3 , the ratio is rather flat and close to 1. This is largely dominated by δ -rays which have nearly the same spectrum for different particle species of the same momentum.

Figure 3 shows the classification performance for various types of truncated mean. The performance is quantified with a receiver operating characteristic (ROC) curve where the probability to correctly tag a kaon is traded off with the probability to incorrectly label a pion as a kaon. The curve traces out various thresholds on the mean dE/dx. The usual truncated mean significantly out-performs the regular mean over all layers for a pion mis-tag rate above about 1%. However, Fig. 2 suggests that maybe truncation is actually too coarse; dE/dx is only unhelpful for values above about 2 MeV cm²/g. Therefore, a second truncation scheme is used whereby all values of dE/dx are used so long as they are less than some threshold θ . This scheme out-performs the truncated mean between 0.1% and about 10% pion mis-tag rates. Figure 3 uses $\theta = 1.8$ MeV cm²/g. A lower threshold value will result in a more symmetric energy loss distribution (unless it is too low), but may throw away potentially valuable information about the spread of the values. This new scheme does introduce a new hyper-parameter; the next section considers taking this to the extreme by trying to approximate the optimal classifier which has many hyper-parameters that can be learned from the simulation (or data).

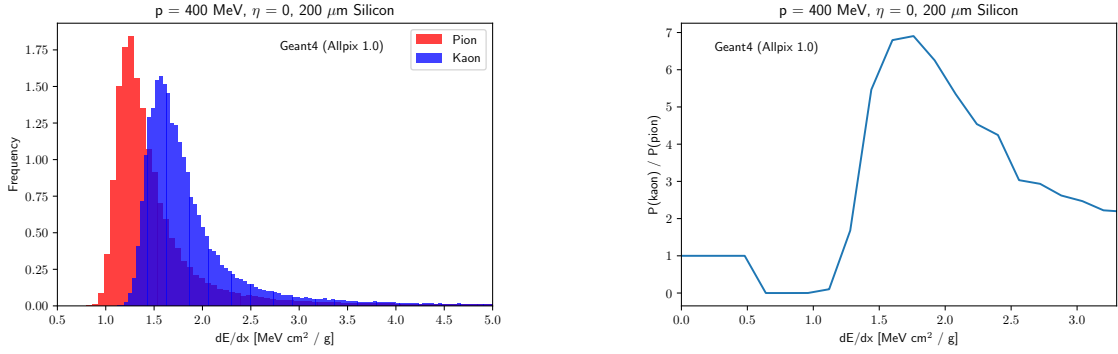


Figure 2: The distribution of energy loss for pion and kaon tracks (left) at a momentum of 400 MeV follows the Landau distribution, with a likelihood ratio (right) which levels off at higher energy loss values.

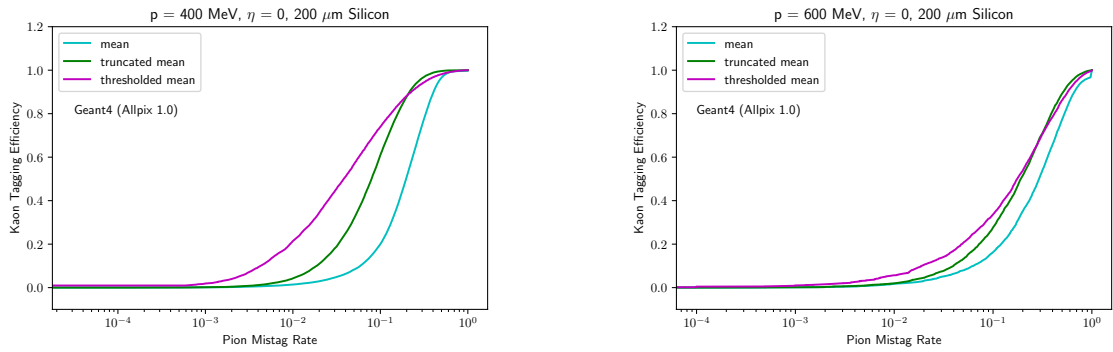


Figure 3: Truncation and thresholding ($\theta = 1.8 \text{ MeV g}^{-1}\text{cm}^2$) provides a significant boost in mean-based classifier performance, shown here at momenta of both 400 MeV (left) and 600 MeV (right).

4 Optimal Classification

In the context of particle identification, each track corresponds to a n -dimensional sample point $\vec{x} \in \mathbb{R}^n$ with a feature representing the energy loss readout (Q_i) for each of the n detector layers:

$$\vec{x} = (Q_1 \quad Q_2 \quad \dots \quad Q_n). \quad (2)$$

The goal of particle identification is to distinguish one process (called S) from another process (called B). For illustration, S will correspond to kaons and B will represent pions. A classifier is a real-valued function h that is optimized to give different values when presented examples of \vec{x} from S and B . The classifier h is optimal if the corresponding ROC curve is no worse than any other classifier, i.e. for any other classifier h' , the probability to misclassify B as S at a fixed signal efficiency for h' is no lower than for h at all possible signal efficiencies. By the Neyman-Pearson lemma [36], an optimal classifier exists and is given by thresholding the likelihood ratio $p_S(\vec{x})/p_B(\vec{x})$, where $p_S(\vec{x})$ is the probability density for \vec{x} for S and similarly for B . For MIPs going through a pixel detector, $p(\vec{x})$ is well-approximated as a product over the probabilities for Q_i in each layer separately. Even with this decomposition, it can be difficult to visualize and validate the optimal classifier in n dimensions and so there is great utility in having a classifier in a reduced feature space where the optimal classifier is specified by a linear decision boundary. Our goal is to both identify the optimal classifier and attempt to find a low-dimensional approximation where a linear threshold is close to optimal.

The optimal classifier for particle identification is estimated using a simple fully connected feed forward artificial neural network (NN). Such NNs are universal function approximators [37] and are empirically known to provide excellent classification performance with a limited training dataset. A one-layer network with 100 neurons and the sigmoid activation function is trained using scikit-learn [38]. Figure 4 shows the performance of the NN trained on the full n -dimensional feature space compared with the optimal classifier using only the truncated mean⁶. Especially for lower momentum particles, the gap between the truncated mean classifier and the optimal classifier is large: for a pion mistag rate of 10%, the optimal classifier has a kaon efficiency of 90% while the truncated mean classifier has a kaon efficiency of 60% at 400 MeV. This performance gap can be nearly eliminated by introducing a measure of spread in addition to the truncated mean. One possibility is to use the truncated standard deviation $\sigma_t(\vec{x})$ of each sample point. As with the truncated mean, the largest value of the sample point is removed before any statistics are calculated in order to account for the large tail of the Landau distribution. A NN trained with only μ_t and σ_t performs nearly the same as one trained on the full sample points as indicated in Fig. 4. This suggests that the reduced two-dimensional feature space contains all of the classification power of the original feature space. In particular, truncation is a nearly lossless operation.

Reducing the original n -dimensional parameter space to two is a significant achievement, but the optimal classifier boundary can still be complicated. It is therefore desirable to

⁶In practice, this is basically the same as a threshold on the truncated mean, but it did not have to be so if the truncated mean was not nearly monotonically related to the likelihood ratio.

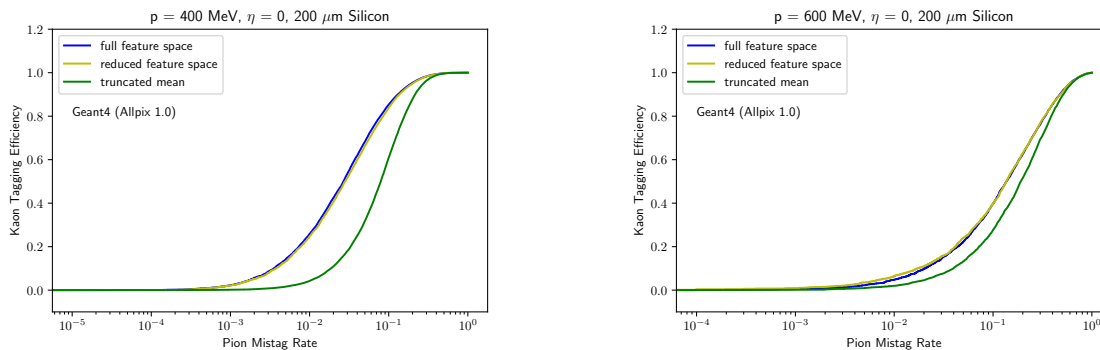


Figure 4: A neural network trained on the full n -dimensional sample points outperforms an optimal classifier trained only with the truncated means. However, a neural network trained on the 2-dimensional feature space consisting of μ_t and σ_t closes this performance gap, shown here at momenta of both 400 MeV (left) and 600 MeV (right).

investigate if a simple transformation can be used to render the optimal classifier linear. The left plot of Fig. 5 shows the ratio of the kaon-to-pion NN output that is trained on μ_t and σ_t . This plot shows that sample points with high average energy loss and low spread in energy loss are the most likely to be classified as kaons, following a decision boundary roughly defined by a quadratic relationship between the truncated mean and truncated standard deviation:

$$\mu_t(\vec{x}) = \sigma_t^2(\vec{x}) + C, \quad (3)$$

where C is a constant. Therefore, a simple threshold on the difference between the truncated standard deviation and truncated variance should create nearly the same decision boundary as a NN trained on the full n -dimensional feature space. The right plot of Fig. 5 shows a ROC curve for the full feature space compared with a simple threshold on Eq. 3. The two curves are nearly identical, which shows that a one-dimensional feature is nearly sufficient to capture all of the relevant information for classification.

Intuition for the optimality of Eq. 3 can be derived from the ideas of sufficient statistics and exponential families [39]. The optimality of truncation was already discussed in the context of δ -rays in Sec. 3. While the energy loss is nearly Landau-distributed, the truncated energy loss is closer to a Gaussian distribution. Classification with Gaussian-distributed random variables only requires the sample mean and sample standard deviation for optimal performance. To see this, note that for a threshold α on the likelihood ratio, the optimal decision boundary for kaons-versus-pions in the Gaussian limit takes the following form:

$$p_\pi(\vec{x}) = \alpha p_k(\vec{x}) \quad (4)$$

$$\frac{1}{(\sqrt{2\pi}\sigma_\pi)^n} \exp\left(-\frac{|\vec{x} - \vec{\mu}_\pi|^2}{2\sigma_\pi^2}\right) = \alpha \left[\frac{1}{(\sqrt{2\pi}\sigma_k)^n} \exp\left(-\frac{|\vec{x} - \vec{\mu}_k|^2}{2\sigma_k^2}\right) \right], \quad (5)$$

where $\vec{\mu}_k, \sigma_k$ are respectively the mean and standard deviation for kaons and analogously

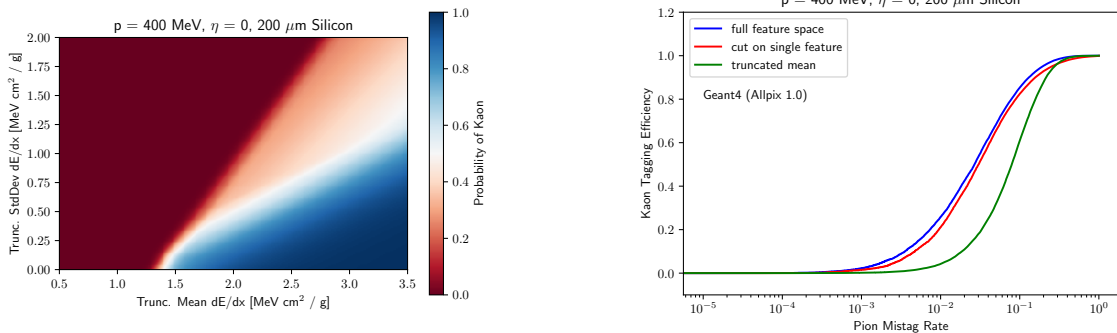


Figure 5: The optimal decision boundary (left) takes the form of a quadratic relationship between $\mu_t(\vec{x})$ and $\sigma_t(\vec{x})$. As a result, a linear cut on the single feature $\mu_t(\vec{x}) - \sigma_t^2(\vec{x})$ performs as well as a neural network trained on the full sample points (right).

$\vec{\mu}_\pi, \sigma_\pi$ are for the defining parameters for pions. Taking the logarithm of both sides and simplifying yields the following:

$$\left(\frac{\mu_\pi}{\sigma_\pi^2} - \frac{\mu_k}{\sigma_k^2} \right) \mu_1(\vec{x}) - \frac{1}{2} \left(\frac{1}{\sigma_\pi^2} - \frac{1}{\sigma_k^2} \right) \mu_2(\vec{x}) = \frac{1}{2} \left(\frac{\mu_\pi^2}{\sigma_\pi^2} - \frac{\mu_k^2}{\sigma_k^2} \right) + \log \frac{\alpha \sigma_\pi}{\sigma_k}, \quad (6)$$

where $\mu_1(\vec{x})$ and $\mu_2(\vec{x})$ denote the first and second raw moments of \vec{x} , respectively. Equation 6 corresponds to a decision boundary of the form $\mu_1(\vec{x}) + w\mu_2(\vec{x}) = b$ for some weight w and bias b determined by the distributions themselves. This resembles the form of Eq. 3. The optimal value of the weight w can further be tuned as another hyper-parameter. For the problem of pion vs kaon classification, we found the optimal value to be near 1.2 g / MeV cm². The change from this weight to the weight of 1 g / MeV cm² used in our approximation causes a negligible decrease in classification power, corresponding to a drop of less than 0.01 in the area under the corresponding ROC curve. Furthermore, the functional form in Eq. 3 continues to be close to optimal even when there are more than four layers, though there is some degradation when there are many more than four layers.

This technique can be extended to identification of tracks from particles besides pions and kaons. We observe similar performance when our model is used to distinguish protons from either pions or kaons (Figure 6).

5 Conclusions

The energy deposited by charged particles in silicon tracking detectors is useful for identifying the particle type when $\beta\gamma < 1$. The truncated mean has been used by many analyses at the LHC and previous experiments. We have shown that truncation is a nearly lossless operation on the set of dE/dx values obtained from multiple tracking layers. However, the truncated mean alone is not sufficient to fully capture all of the available information. By adding a measure of spread as a second feature, we are able to achieve the optimal classification. A simple difference of the truncated mean and variance is nearly sufficient to fully capture all of

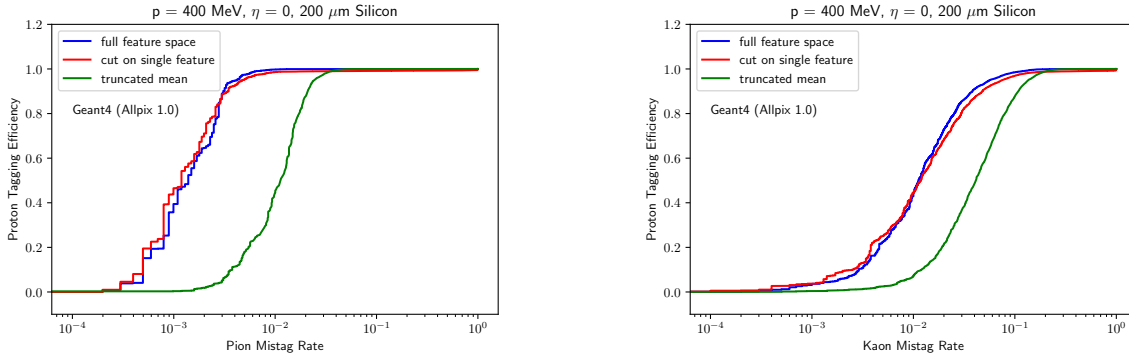


Figure 6: A linear cut on the single feature $\mu_t(\vec{x}) - \sigma_t^2(\vec{x})$ matches the performance of a neural network trained on the full sample points for both the tasks of distinguishing protons from pions (left) and from kaons (right).

the available information. Similar results are observed when varying the particle momentum as well as the particle types. Hopefully the techniques developed here will be useful for fully exploiting the data at the LHC for both measurements of fragmentation and other quantum chromodynamical processes as well as searches for new particles beyond the Standard Model that are charged and slow moving.

6 Acknowledgments

We would like to thank Maurice Garcia-Sciveres for comments on the manuscript. This work was supported by the U.S. Department of Energy, Office of Science under contract DE-AC02-05CH11231.

References

- [1] ATLAS Collaboration, The ATLAS Experiment at the CERN Large Hadron Collider, JINST 3 (2008) S08003.
- [2] ATLAS Collaboration, dE/dx measurement in the ATLAS Pixel Detector and its use for particle identification, ATLAS-CONF-2011-016.
- [3] CMS Collaboration, The CMS Experiment at the CERN LHC, JINST 3 (2008) S08004.
- [4] CMS Collaboration, CMS Tracking Performance Results from early LHC Operation, Eur. Phys. J. C70 (2010) 1165–1192. [arXiv:1007.1988](#).
- [5] ALICE Collaboration, The ALICE experiment at the CERN LHC, JINST 3 (2008) S08002.
- [6] ALICE Collaboration, Performance of the ALICE Experiment at the CERN LHC, Int. J. Mod. Phys. A29 (2014) 1430044. [arXiv:1402.4476](#).
- [7] LHCb Collaboration, The LHCb Detector at the LHC, JINST 3 (2008) S08005.
- [8] LHCb Collaboration, Performance of the LHCb Vertex Locator, JINST 9 (2014) 09007. [arXiv:1405.7808](#).
- [9] C. Parkes, T. Ruf, T. Szumlak, Reconstruction of Cluster Positions in the LHCb Velo, LHCb-2007-151.
- [10] G. D. McGregor, Calibration of the LHCb VELO Detector and Study of the Decay Mode $D^0 \rightarrow K^- \mu^+ \nu_\mu$, CERN-THESIS-2011-152.
- [11] ATLAS Collaboration, Performance of the ATLAS Transition Radiation Tracker in Run 1 of the LHC: tracker properties, JINST 12 (2017) P05002. [arXiv:1702.06473](#).
- [12] CMS Collaboration, Study of the inclusive production of charged pions, kaons, and protons in pp collisions at $\sqrt{s} = 0.9, 2.76, \text{ and } 7 \text{ TeV}$, Eur. Phys. J. C72 (2012) 2164. [arXiv:1207.4724](#).
- [13] CMS Collaboration, Study of the production of charged pions, kaons, and protons in pPb collisions at $\sqrt{s_{NN}} = 5.02 \text{ TeV}$, Eur. Phys. J. C74 (2014) 2847. [arXiv:1307.3442](#).
- [14] CMS Collaboration, Study of Bose-Einstein correlations in pp, pPb, and PbPb collisions at the LHC, [arXiv:1712.07198](#).
- [15] ATLAS Collaboration, Search for metastable heavy charged particles with large ionization energy loss in pp collisions at $\sqrt{s} = 13 \text{ TeV}$ using the ATLAS experiment, Phys. Rev. D93 (2016) 112015. [arXiv:1604.04520](#).
- [16] CMS Collaboration, Search for long-lived charged particles in proton-proton collisions at $\sqrt{s} = 13 \text{ TeV}$, Phys. Rev. D94 (2016) 112004. [arXiv:1609.08382](#).

- [17] ATLAS Collaboration, Searches for heavy long-lived charged particles with the ATLAS detector in proton-proton collisions at $\sqrt{s} = 8$ TeV, JHEP 01 (2015) 068. [arXiv:1411.6795](#).
- [18] CMS Collaboration, Searches for long-lived charged particles in pp collisions at $\sqrt{s}=7$ and 8 TeV, JHEP 07 (2013) 122. [arXiv:1305.0491](#).
- [19] ATLAS Collaboration, Search for stable hadronising squarks and gluinos with the ATLAS experiment at the LHC, Phys. Lett. B701 (2011) 1. [arXiv:1103.1984](#).
- [20] ATLAS Collaboration, Searches for heavy long-lived sleptons and R-Hadrons with the ATLAS detector in pp collisions at $\sqrt{s} = 7$ TeV, Phys. Lett. B720 (2013) 277. [arXiv:1211.1597](#).
- [21] ATLAS Collaboration, Search for long-lived, multi-charged particles in pp collisions at $\sqrt{s}=7$ TeV using the ATLAS detector, Phys. Lett. B722 (2013) 305–323. [arXiv:1301.5272](#).
- [22] CMS Collaboration, Search for heavy long-lived charged particles in pp collisions at $\sqrt{s} = 7$ TeV, Phys. Lett. B713 (2012) 408. [arXiv:1205.0272](#).
- [23] CMS Collaboration, Search for Heavy Stable Charged Particles in pp collisions at $\sqrt{s} = 7$ TeV, JHEP 03 (2011) 024. [arXiv:1101.1645](#).
- [24] H. Bichsel, A method to improve tracking and particle identification in TPCs and silicon detectors, Nucl. Instrum. Meth. A562 (2006) 154.
- [25] C. Patrignani, et al., Review of Particle Physics, Chin. Phys. C40 (2016) 100001.
- [26] J. Idarraga, M. Benoit, Generic Geant4 implementation for pixel detectors, The AllPix Simulation Framework (2006) [[twiki.cern.ch:AllPix](#)].
- [27] GEANT4 Collaboration, GEANT4: A Simulation toolkit, Nucl. Instrum. Meth. A506 (2003) 250–303.
- [28] Y. Chen, et al., Optimal use of Charge Information for the HL-LHC Pixel Detector Readout, Nucl. Instrum. Meth. A (2018), [arXiv:1710.02582](#).
- [29] F. Wang, et al., The Impact of Incorporating Shell-corrections to Energy Loss in Silicon, [arXiv:1711.05465](#).
- [30] A. Fick, Ueber diffusion, Annalen der Physik 170 (1855) 59.
- [31] W. Sutherland, A dynamical theory of diffusion for non-electrolytes and the molecular mass of albumin, The London, Edinburgh, and Dublin Philosophical Magazine and Journal of Science 9 (1905) 781.
- [32] A. Einstein, Über die von der molekularkinetischen theorie der wrme geforderte bewegung von in ruhenden flüssigkeiten suspendierten teilchen, Annalen der Physik 322 (1905) 549.

- [33] M. von Smoluchowski, Zur kinetischen theorie der brownschen molekularbewegung und der suspensionen, *Annalen der Physik* 326 (1906) 756.
- [34] D. Caughey, R. Thomas., Carrier Mobilities in Silicon Empirically Related to Doping and Field., *Proc. IEEE* 55 (1967) 2192.
- [35] C. Canali, et al., Electron and hole drift velocity measurements in silicon and their empirical relation to electric field and temperature, *IEEE Trans. Electron Devices* 22 (1975) 1045.
- [36] J. Neyman, E. S. Pearson, On the problem of the most efficient tests of statistical hypotheses, *Phil. Trans. R. Soc. Lond. A* 231 (1933) 289.
- [37] K. Hornik, Approximation capabilities of multilayer feedforward networks, *Neural Networks* 4 (1991) 251.
- [38] F. Pedregosa, et al., Scikit-learn: Machine learning in Python, *Journal of Machine Learning Research* 12 (2011) 2825.
- [39] R. A. Fisher, On the mathematical foundations of theoretical statistics, *Phil. Trans. R. Soc. Lond. A* 222 (1922) 309.